Journal of Materials Processing Tech. 293 (2021) 117080

Contents lists available at ScienceDirect

Journal of Materials Processing Tech.

journal homepage: www.elsevier.com/locate/jmatprotec

Wire based plasma arc and laser hybrid additive manufacture of Ti-6Al-4V

Chong Wang *, Wojciech Suder, Jialuo Ding, Stewart Williams

Welding Engineering and Laser Processing Centre, Cranfield University, Bedfordshire, MK43 0AL, UK

ARTICLE INFO

Associate Editor: R Mishra

Keywords:
Plasma arc-laser hybrid additive manufacture
Wire + arc additive manufacture
Wire + laser additive manufacture
High deposition rate
Multi-energy source

ABSTRACT

In this study, a novel wire based plasma transferred arc (PTA)-laser hybrid additive manufacture process was proposed for deposition of large-scale titanium parts with high deposition rate and near-net shape. The optimum processing conditions, including the heat source configuration, wire feeding position, and arc-to-laser separation distance, were investigated. The benefits of using the hybrid process over the single PTA and laser deposition processes on their own were studied. The results show that compared to the single PTA process, the hybrid process has extended energy distribution and melt pool size, giving more interaction time of the wire with the heat sources and therefore a higher deposition rate. Compared to the laser process, the hybrid process has a much higher wire melting efficiency and tolerance to wire positioning accuracy. Owing to more distributed energy across the two heat sources, the likelihood of keyhole formation in the hybrid process is lower than that in the single PTA process. The best configuration for the hybrid process is the PTA leading, combined with front feeding of the wire. In this configuration, the PTA is used to melt the feedstock and the laser is used to control the melt pool size, which allows independent control of deposition rate and bead shape. A set of multi-layer walls was built to demonstrate the feasibility of this process for the manufacture of engineering parts. The results show that the achieved flat beads are very desirable for low surface waviness and lead to near-net-shape deposition. The main limitation of the hybrid process is remelting into the underlying layer. To overcome this, a multi-energy source process with more evenly distributed energy has been proposed.

1. Introduction

Directed energy deposition (DED) additive manufacture (AM) has developed rapidly due to advantages such as short lead-times compared to forgings, low material waste compared to machining, and high design flexibility, as described by Singh et al. (2020). Wire based DED AM processes have much higher deposition rates and lower material waste in comparison with powder based processes, leading to the potential to produce large-scale and near-net-shape metallic components in many industry sectors, including aerospace, aviation, and power generation, as stated by Cong et al. (2017) and Qi et al. (2018). Depending on the heat source, there are three principal types of wire based DED AM processes, which are electron beam freeform fabrication (EBF^3), wire + laser additive manufacture (WLAM), and wire + arc additive manufacture (WAAM). EBF^3 is conducted in a vacuum chamber, resulting in relatively high equipment cost, low duty cycles, long cooling times, and therefore is not widely used. In WLAM, near-net-shape components can be achieved due to the independent control of laser power and power distribution (principally beam size) which allows achievement of stable melting without keyhole formation, as demonstrated by Baufeld et al. (2011). However, due to the low absorptivity of lasers in many metals, very high laser powers are required for high build rates in the WLAM process. This leads to much higher costs, and there is a lot of reflected power to manage. In WAAM, using the plasma transferred arc (PTA) process, reasonable deposition rates can be achieved (e.g. 1 kg/h for titanium) due to the high energy transfer efficiency of the electric arc compared to lasers, making large-scale parts achievable in reasonable times (Williams et al., 2016). In principle, it is possible to further increase the deposition rate in the PTA process but, unlike the WLAM process, it is impossible to greatly vary the energy distribution. Therefore, the high current required for higher deposition rates increases the likelihood of keyhole formation due to high arc pressure, which limits the deposition rate, as stated by Wang et al. (2021). Comparing WLAM and WAAM processes, one can see that each process has its own advantages and disadvantages. Therefore, a wire based PTA-laser hybrid AM process was investigated to combine the advantages of both heat sources and thus to build parts with higher deposition rates, no defects, and near-net shape.

* Corresponding author.
E-mail address: chong.wang1@cranfield.ac.uk (C. Wang).

https://doi.org/10.1016/j.jmatprotec.2021.117080
Received 5 November 2020; Received in revised form 18 January 2021; Accepted 30 January 2021
Available online 4 February 2021
0924-0136/© 2021 The Authors. Published by Elsevier B.V. This is an open access article under the CC BY license (http://creativecommons.org/licenses/by/4.0/).

For arc-laser hybrid AM, there have been only a few research papers published in the past few years, and most of them are based on gas metal arc (GMA) process. This is because the GMA process has higher tolerance in path planning and omnidirectionality than gas tungsten arc (GTA) and PTA, owing to the coaxial configuration of the consumable electrode (i.e. wire) and torch. Besides, it has relatively high deposition rates. For example, a deposition rate of 3 kg/h is easy to achieve for steel with a single GMA heat source (Williams et al., 2016). The deposition rate can be up to 9.5 kg/h for steel in a Tandem process (Martina et al., 2019). Näsström et al. (2019a,2019b) investigated cold metal transfer (CMT) arc-laser hybrid AM process of steel, and compared the deposited components obtained with only CMT, CMT with leading laser, and CMT with trailing laser. They found that the CMT arc with trailing laser configuration improved the process stability and consequently improved the surface finish and geometric feature capability. Pardal et al. (2019) studied the benefits of introducing a concentric laser as a secondary heat source in CMT based WAAM of titanium. Compared to the CMT process alone, the hybrid process stabilised the arc, leading to an improved bead shape, as well as a higher deposition rate. Zhang et al. (2018) investigated GMA-laser hybrid AM of aluminium and obtained similar results. They found that compared to GMA process, the surface quality of the components was improved significantly by adding a laser, and the efficiency of material utilisation was increased by 15 %. It is noteworthy that the above studies focused mainly on improving the surface finish of the GMA based deposition process by adding the laser. This is because the GMA process with a consumable electrode is not very stable, as revealed by Modenesi and Nixon (1994), which results in relatively rough surface finish. In addition, in some materials with a low work function such as titanium, the cathode spot is not fixed on one point and electrons can be extracted from a large area, leading to arc wandering (Pardal et al., 2019). Besides, the high surface tension of titanium leads to difficulties with droplet detachment as well as large spatter in the GMA process. Hence, it is difficult to deposit titanium with GMA process. However, in arc processes with a non-consumable electrode such as GTA and PTA, the electrons are emitted from the tungsten electrode (thermionic emission) and the arc is stable, which are suitable for deposition of titanium.

Miao et al. (2020) compared the microstructure and mechanical properties of aluminium parts deposited by both the GTA-laser hybrid deposition process and GTA based deposition process. They found that the addition of the laser led to more uniform element distribution and finer grains caused by the strengthened fluid flow and high cooling rate in the laser-affected zone. This resulted in an improved hardness and strength of the samples. Wu et al. (2020) studied the microstructure and mechanical properties of Al-Cu alloy deposited by GTA-laser hybrid AM process and stated that the grain size is smaller and Cu element distributes more homogenously in the laser-arc-affected zone compared to the arc-affected zone in each layer. It can be concluded that most of the published studies about the arc-laser hybrid AM are mainly focused on surface quality or material characterisation. However, how the energy of laser and arc affects the feedstock melting (efficiency and deposition rate) and melt pool control (remelting and bead shape) has not been reported, which is of vital significance to improve the deposition rate and final shape of the deposited components. In addition, compared to the GTA based process, the PTA based process has a higher stand-off distance due to the more concentrated arc column, which gives a higher tolerance in terms of wire feeding position and layer height errors. Therefore, the PTA-laser hybrid AM process is expected to give more benefits than the GTA based hybrid AM process.

In this study, a PTA-laser hybrid AM process was investigated for the deposition of Ti-6Al-4V. The optimum processing conditions, including the configuration of the laser and PTA heat sources, wire feeding direction, wire feeding position, and arc-laser separation distance, were studied. The benefits of using the hybrid process over PTA and laser processes on their own in terms of improved efficiency and deposition rate were investigated. Three multi-layer single-pass walls were deposited to evaluate the geometric quality of the parts and to study the limitations of the standard hybrid deposition process. A further adaptation of the arc-laser hybrid concept was developed to overcome the observed limitations. This is a multi-energy source (MES) approach utilising three heat sources (one PTA and two separate lasers).

2. Experimental procedure

2.1. Materials and setup

Ti-6Al-4V wire with a diameter of 1.2 mm was used as the feedstock material, and Ti-6Al-4V plate with dimensions of 300 mm × 200 mm × 7 mm was used as the substrate. The PTA was generated by a EWM Tetrix 552 power supply. Pure argon was used for both plasma gas and shielding gas for the plasma torch with the flowrates of 0.8 and 8 L/min, respectively. The tungsten electrode had a diameter of 4 mm with a tip angle of 40° and a set-back of 2.4 mm. The copper orifice had a diameter of 3.9 mm, and the stand-off distance between the orifice and workpiece was 8 mm. A continuous-wave fibre laser (IPG YLR-8000, wavelength: 1.07 μm) with a maximum power of 8 kW was used for the laser source. The laser is delivered through a fibre with a core diameter of 0.3 mm, and the focal lengths of the collimation lens and focusing lens are 125 and 250 mm respectively. The optical setup gives a laser beam with a focal spot diameter of 0.6 mm. The laser defocusing was applied during all depositions.

Fig. 1 shows the experimental setup for the PTA-laser hybrid AM system. The deposition was conducted in an enclosed tent to prevent the material from oxidation, which was purged with argon until the oxygen level was below 500 ppm as verified by an oxygen analyser. A 6-axis Fanuc robot was used to provide motion for the system, and the robot's end-effector was enclosed in the tent. A Dinse wire feeder was used to feed the wire. The arc current and voltage were recorded by an arc monitor (Triton Electronics AMV4000). The plasma torch was inclined at an angle of 20° to protect it from the burning by the laser beam. The laser head was inclined at an angle of 30° to prevent back reflection. The deposition process, including the metal transfer and melt pool behaviour, was monitored using a CMOS process camera (Xiris XVC-1000).

2.2. Methods

2.2.1. Processing conditions in the hybrid process

As shown in Fig. 2, two different configurations regarding the relative position of the wire, plasma torch, and laser head were used, in which the wire was either irradiated by the PTA first (Fig. 2a) or by the laser first (Fig. 2b). Note that the wire feeding angles were slightly different in the two configurations to feed the wire properly. When considering the wire feeding direction, there are four configurations for the wire and heat sources: wire front feeding with PTA leading (a1), wire back feeding with laser leading (a2), wire front feeding with laser leading (b1), and wire back feeding with PTA leading (b2). Based on the outcome of initial optimisation (explained in Section 3.1.1), the configuration with wire front feeding and PTA leading (a1) was used for the remaining experiments. It should be noted that the substrate was fixed during all the deposition. Therefore, the travel direction mentioned in this study is based on the movement of the plasma torch and laser head.

To investigate the tolerance of the hybrid process to wire positioning accuracy and process robustness, some deposits were conducted with different wire feeding positions. In this procedure, the distance (d_1) between the wire tip and workpiece was increased from 0 to 4 mm with an increment of 1 mm. The wire melting and melt pool behaviour were recorded by the process camera. To study the effect of the separation distance between the heat sources on the deposition process and bead appearance, a set of beads was deposited by increasing the arc-laser separation distances (d_2) from 10 to 18 mm with an increment of 2 mm. The definition of d_1 and d_2 is illustrated in Fig. 3. The distances of d_1

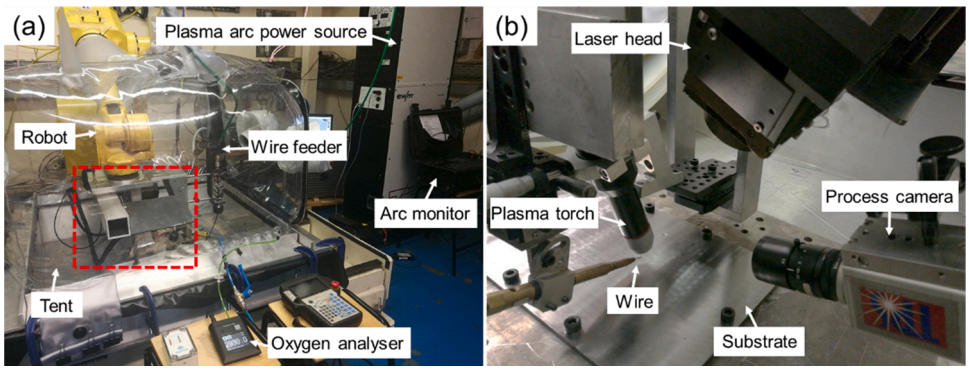


Fig. 1. (a) Experimental setup for PTA-laser hybrid AM system, and (b) view from inside of the tent, which is indicated by a red dashed square in (a) (For interpretation of the references to colour in this figure legend, the reader is referred to the web version of this article.).

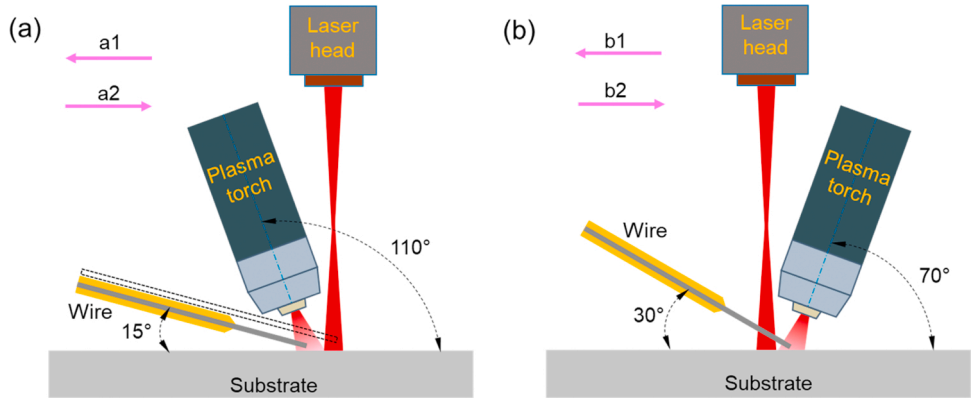


Fig. 2. Different configurations and travel directions (indicated by pink arrows) used: (a) the wire is first irradiated by the PTA, and (b) the wire is first irradiated by the laser.

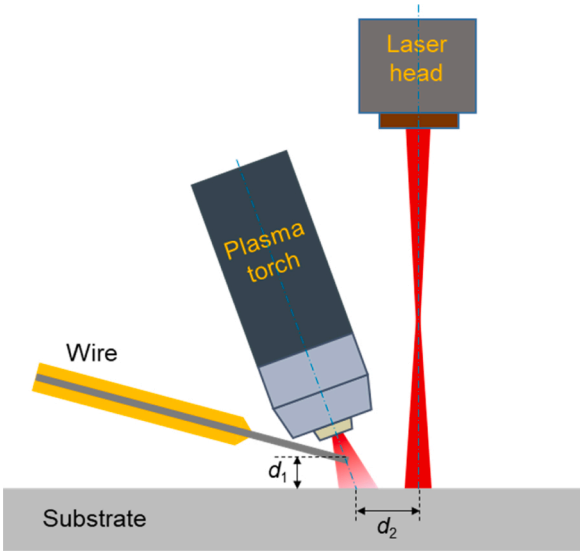


Fig. 3. Illustration of the definition of d_1 and d_2.

and d_2 were not changed during deposition, and they were varied using two separate manual linear stages before each deposit was conducted. Table 1 shows the parameters that were maintained constant.

2.2.2. Deposition rate in different AM processes

The deposition rate, R, is expressed by:

Table 1
Fixed process parameters used during the experiments.

Parameters	Value (unit)
Travel speed (TS)	4.5 mm/s
Wire feed speed (WFS)	4 m/min
Laser beam diameter	12 mm
Arc current	200 A

$$R = \frac{\pi d^2 v_w \rho}{4} \quad (1)$$

where d is the wire diameter, v_w is WFS, ρ is the density of the wire. Therefore, for a given wire, the deposition rate is only controlled by WFS. First, the limit of deposition rate for the same applied power was achieved for each process separately, i.e. PTA and laser. In each case, a maximum WSF was found at a given power, above which the wire could not be melted anymore, established from the video recordings. The power was increased from 2 to 8 kW with an increment of 2 kW. Next, the deposition rate of the hybrid process was compared with those of laser and PTA on their own for the same power output of 8 kW. In the hybrid process, the ratio between the laser power and the PTA power was varied but for a constant total power of 8 kW. For each ratio, the maximum WFS was recorded and compared. It should be mentioned that in this series of experiments, the wire feeding position was lifted up to make sure that both the PTA and laser can irradiate on the wire, which is indicated by the dashed outline as shown in Fig. 2a.

In order to achieve the exact power needed from the PTA power supply, several deposits were conducted with different currents, where the current and voltage were recorded by arc monitor. The output power

of the power supply, Q, is given by:

$$Q = UI \tag{2}$$

where U and I are arc voltage and current, respectively. Based on Eq. (2) and the data obtained from the arc monitor, the output power of the PTA as a function of current was obtained, as shown in Fig. 4.

2.2.3. Tolerance of WLAM

To compare the tolerance of the hybrid process with WLAM process in terms of wire positioning accuracy, some additional deposits were conducted with WLAM. In this case, the distance from the wire tip to the substrate was increased from 0 to 4 mm with an increment of 1 mm. The WFS and TS used were 2 m/min and 4.5 mm/s, respectively. A 4 kW laser power with a defocused laser beam diameter of 8 mm was used.

2.2.4. Limitation of WAAM

To study the limit of WAAM process due to keyhole formation, some experiments with varying power input and deposition rate were conducted with WAAM and hybrid processes. In the wire based AM processes, the ratio of WFS to TS is an important parameter, which determines the cross-sectional area of the bead. During the deposition, if we neglect vaporisation of the material or spatter, the volume of melted wire and the deposited bead will be the same. In a unit time, they can be expressed by the following equation:

$$\frac{\pi d^2}{4} v_w = \mathrm{A} v_t \tag{3}$$

where A is the cross-sectional area of the bead (not including the remelting area, as shown in Fig. 5), and v_t is TS. From Eq. (3), the ratio of WFS to TS can be expressed as follows:

$$\frac{v_w}{v_t} = \frac{4\mathrm{A}}{\pi d^2} \tag{4}$$

It can be seen that for a given wire diameter, the WFS to TS ratio is proportional to the cross-sectional area (A) of the bead. Note that the ratio of the bead area (A) to the remelting area (B) is the remelting ratio, and the dilution is given by B/(A + B).

In order to achieve the same bead shape (i.e. bead height and bead width) with different processes, the WFS to TS ratio should be the same. In addition, the heat input per unit length should be the same. Therefore, the WFS and TS were increased proportionally to achieve higher deposition rates (controlled by WFS). Meanwhile, the heat input was increased proportionally from a low value to a limit value marked by the onset of keyhole formation. The experiment was first conducted for WAAM and then compared with the hybrid process.

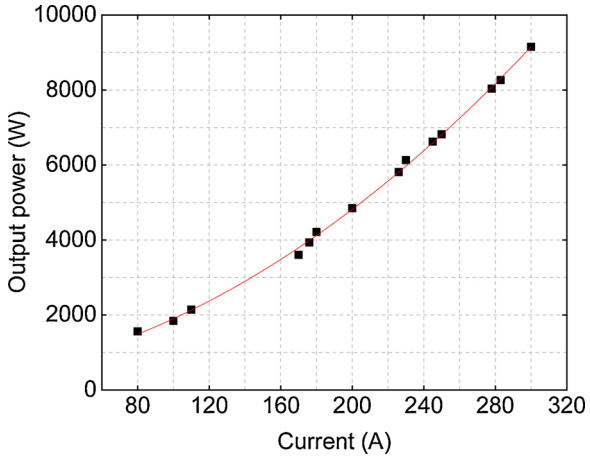


Fig. 4. Measured output power of PTA as a function of applied current.

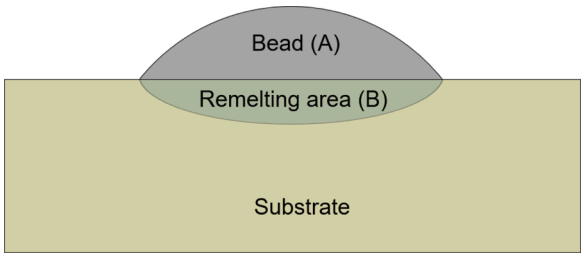


Fig. 5. Schematic diagram of the deposited bead with a cross-sectional area of A and remelting area of B.

2.2.5. Multi-layer wall building

To evaluate the geometric quality of the components deposited by the hybrid process, three multi-layer single-pass walls were deposited at different deposition rates. The process parameters used are listed in Table 2. The parts were cross-sectioned, mounted, polished, and etched after being deposited to check the profile and surface waviness.

2.2.6. Multi-energy source deposition

In AM, the deposition process efficiency can be reflected by the energy needed for deposition of per unit mass of material, which is defined by:

$$e = \frac{P}{R} \tag{5}$$

where P is the total applied power of the process, and R is the deposition rate. It can be seen that the lower the value of e, the higher the deposition process efficiency. The initial results show that with the standard PTA-laser hybrid configuration, the remelting ratio is high, resulting in low deposition process efficiency (explained in Section 3.3). To overcome the low process deposition efficiency and reduce the remelting depth of the process, the energy distribution needs to be adjusted so that more energy is applied to the edges of the melt pool generated by the PTA. To achieve this, we investigated a MES concept (Williams and Suder, 2021), where three or more energy sources are combined to give an adaptable and optimised power density profile. The specific arrangement used for this initial investigation is shown in Fig. 6. The PTA source was leading, and two laser sources were placed at the edges of the melt pool. The distance between the two lasers was 8 mm. Due to the practical limitations of this complex setup, back wire feeding was used.

To compare the benefits of using MES over the standard hybrid process, a deposit was also conducted using the standard PTA-laser hybrid process. In both configurations, the WFS, TS, arc current and the total applied power of laser are the same except for the laser energy distribution. All the parameters used for the two processes are shown in Table 3.

3. Results and discussion

3.1. Processing conditions of the hybrid AM

3.1.1. Configuration

Fig. 7 shows the hybrid deposition processes with front feeding

Table 2
Process parameters used for deposition of the multi-layer single-pass walls.

Parameters (unit)	Wall 1	Wall 2	Wall 3
TS (mm/s)	4.5	4.5	4.5
WFS (m/min)	4	6	8
Arc current (A)	200	240	280
Laser beam diameter (mm)	12	12	12
Laser power (kW)	3	5	5

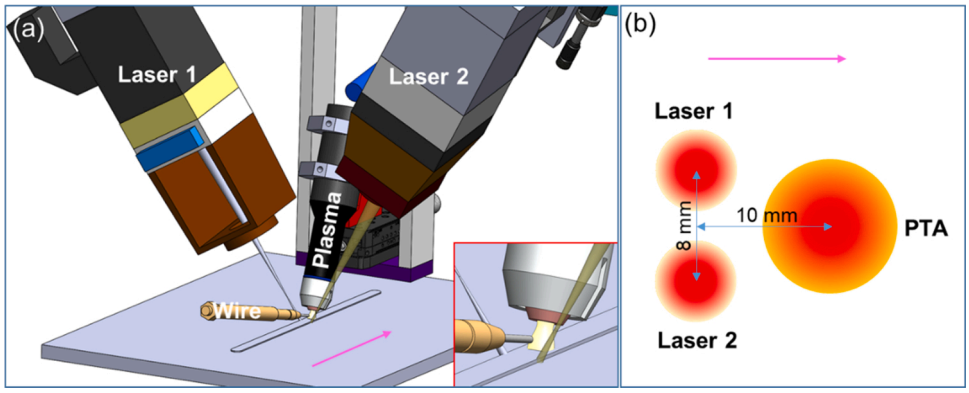


Fig. 6. Schematic shows (a) the configuration of MES with one PTA and two separate lasers, and (b) the relative position of the three energy sources. Pink arrows indicate the travel direction.

Table 3
Process parameters used for the standard PTA-laser hybrid process and MES deposition process.

Parameters (unit)	Standard hybrid process	MES
TS (mm/s)	4.5	4.5
WFS (m/min)	4	4
Arc current (A)	200	200
Laser beam diameter (mm)	12	Laser 1: 6 Laser 2: 6
Laser power (kW)	3	Laser 1: 1.5 Laser 2: 1.5

configurations. In Fig. 7a, the PTA was leading. It can be seen that the wire was melted by the PTA with small droplets being transferred into the melt pool. The laser was placed behind the PTA to make the bead wider by adding more power into the melt pool. The small droplets appear to be in continuous contact with the melt pool, ensuring smooth metal transfer. This resulted in a wide and smooth bead, as shown in Fig. 7c. In contrast, large droplets generated in the laser leading configuration, which resulted in a less smooth bead with large ripples on the surface, as shown in Fig. 7d. The high laser power, in this case, was sufficient to melt the wire. However, as shown in Fig. 7b, the high surface tension of titanium and the lack of arc pressure that would push the droplets towards the melt pool resulted in large droplets with a lower detachment frequency.

In the first case (Fig. 7a), the stable metal transfer was attributed to the arc pressure produced by PTA, which pushed the small droplet into the melt pool regularly. In the second case (Fig. 7b), however, there was no detachment force for the droplet when the wire was melted. Therefore, the droplet kept growing and detached from the wire only when touching the melt pool. In this case, the gravitational force and the surface tension from the melt pool were the main detachment forces. The large droplets with low detachment frequency in the second case induced oscillations in the melt pool. Therefore the configuration with the wire being melted by the PTA is more suitable for the hybrid process.

Fig. 8 shows the hybrid deposition process where the arc pressure is used to transfer the metal from the wire. As indicated by the blue arrow in Fig. 8a, the contact tip is in very close proximity to the deposited bead when the wire is in the back feeding position, leading to a lower tolerance in wire position compared to the front feeding position shown in Fig. 8b. Therefore, the configuration of wire front feeding with PTA leading was selected for further experiments.

3.1.2. *Wire feeding position*

Fig. 9 shows the hybrid deposition process with different wire feeding positions with respect to the surface of the workpiece, and Fig. 10 shows the bead appearance and bead width obtained with the corresponding positions. When the wire feeding position was too low (d_1 = 0, Fig. 9a), the wire stabbed the workpiece before it could be fully

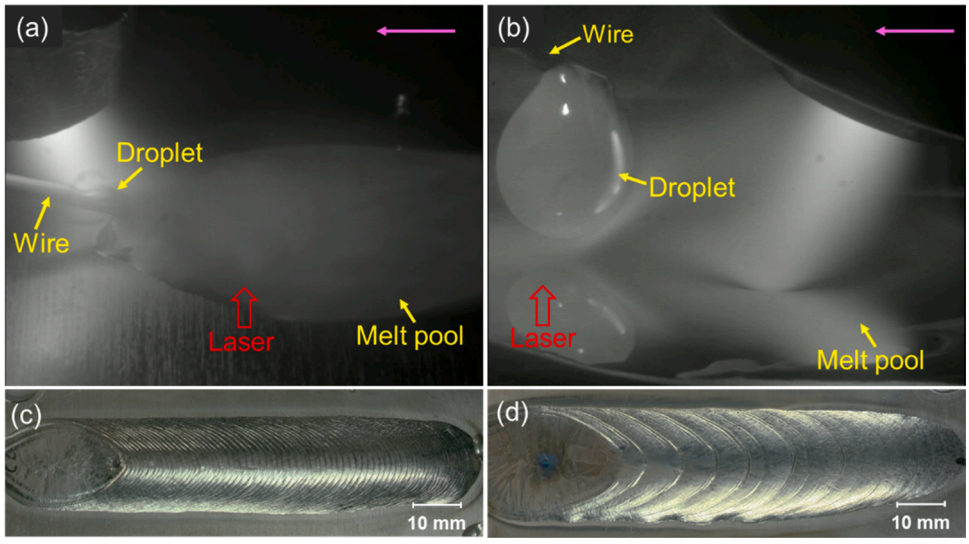


Fig. 7. The effect of wire orientation and leading source on the deposition process and bead appearance for 7 kW laser and 200 A current: (a) wire melted by the PTA, and (b) wire melted by the laser. (c) and (d) show the bead appearances obtained with the processes in (a) and (b), respectively.

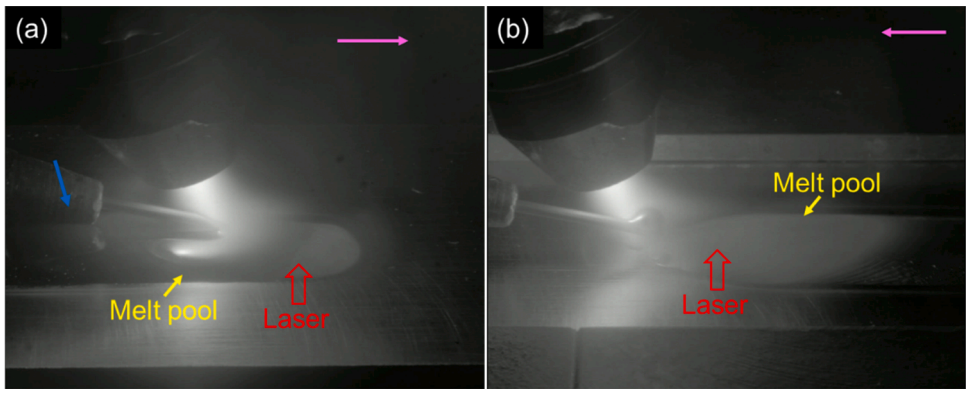


Fig. 8. The effect of wire feeding direction on the hybrid deposition process: (a) back feeding, and (b) front feeding. The laser power used in both cases was 3 kW.

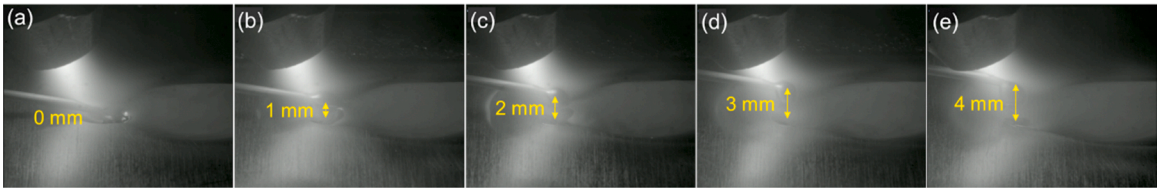


Fig. 9. The effect of wire-workpiece distance on the deposition process: (a) $d_1 = 0$, (b) $d_1 = 1$ mm, (c) $d_1 = 2$ mm, (d) $d_1 = 3$ mm, and (e) $d_1 = 4$ mm.

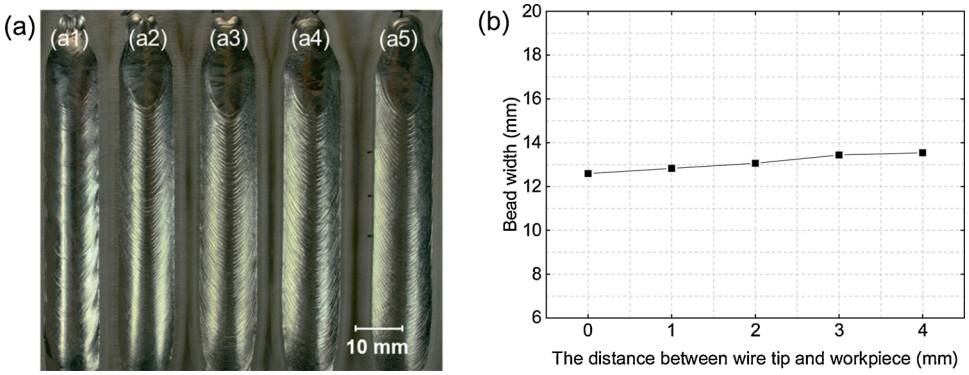


Fig. 10. (a) Bead appearance and (b) bead width obtained with different wire-workpiece distances: (a1) $d_1 = 0$, (a2) $d_1 = 1$ mm, (a3) $d_1 = 2$ mm, (a4) $d_1 = 3$ mm, and (a5) $d_1 = 4$ mm.

melted, increasing the likelihood of bending and misaligning of the wire. The bead obtained with this process is shown in Fig. 10(a1), which had irregular edges. However, when the wire feeding position became higher (from 1 to 4 mm), the metal was transferred to the metal pool in regular intervals, which led to a good bead appearance, as shown in Fig. 10(a2-a5). It also can be seen from Fig. 10b that the bead width increases very slightly (from 12.83 to 13.54 mm) as the wire feeding position changes from 1 to 4 mm. Wang et al. (2021) studied the effect of wire feeding position on the bead shape and metal transfer behaviour and stated that the increased bead width with higher wire feeding position is attributed to the improvement in melting efficiency. With the low position, some of the wire is melted in the melt pool, leading to much energy taken from the melt pool by the wire and therefore a narrower bead. When the position is higher, all the wire is melted in the arc, resulting in higher process efficiency and wider bead. In general, it can be concluded that the hybrid process has a high tolerance to the wire feeding position since the metal transfer behaviour and the bead shape did not change significantly when the distance between wire tip and workpiece changed from 1 to 4 mm.

In addition, the beads deposited by the hybrid process have smooth surface even for settings of wire where large droplets are formed. For example, even when the droplets impact the melt pool with high energy from a high position ($d_1 = 4$ mm), the melt pool was still stable (Fig. 9e), and the bead surface was smooth (Fig. 10(a5)). This is because the wire is melted by PTA, which takes advantage of the high tolerance of PTA and the additional energy from the laser then expands and stabilises the melt pool, which means that any oscillations in the melt pool dampen down before the onset of solidification.

3.1.3. *Arc-laser separation distance*

Fig. 11 shows the deposition process with different separation distances between PTA and laser, and Fig. 12 shows the corresponding bead appearances and bead widths. It can be seen from Fig. 11a that when the two heat sources were relatively close to each other ($d_2 = 10$ mm), there was just one common melt pool formed. However, when the separation distance increased to 14 mm (Fig. 11c), a clear narrowing with two separated melt pools could be observed. This means that the melt pool generated by the PTA lost a significant amount of energy and almost solidified before the laser impinged on it. As the separation distance further increased (Fig. 11d and 11e), the gap between the two melt pools became larger. It should be noted that this effect is dependent on the energy and spot size of the laser and PTA.

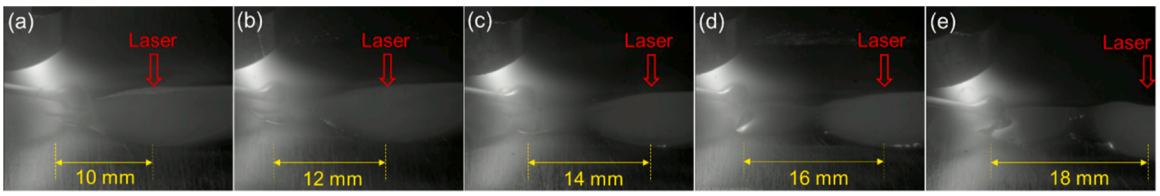


Fig. 11. The effect of arc-laser separation distance on the deposition process: (a) $d_2 = 10$ mm, (b) $d_2 = 12$ mm, (c) $d_2 = 14$ mm, (d) $d_2 = 16$ mm, and (e) $d_2 = 18$ mm.

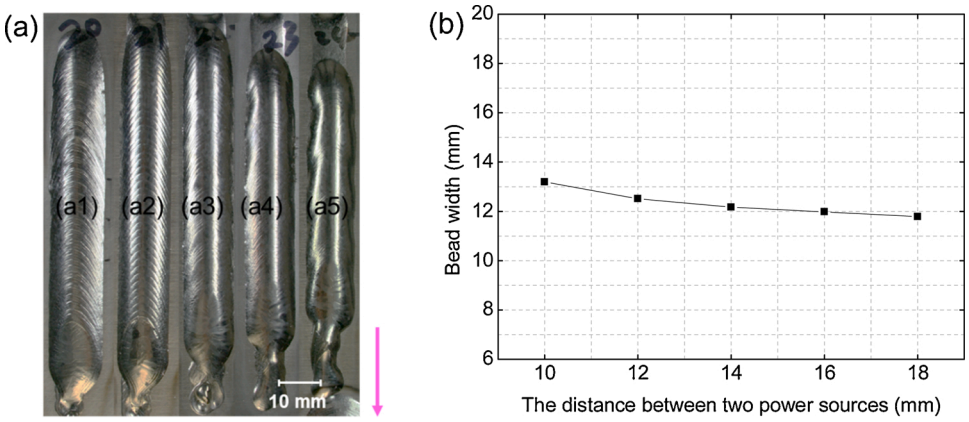


Fig. 12. The effect of arc-laser separation distance on (a) bead appearance, and (b) bead width. The pink arrow indicates the deposition direction.

It can be seen from Fig. 12a that the separation distance also affects the final bead shape. The beads are irregular when two separated melt pools are formed, and this becomes worse as the separation distance increases. Also, beyond a certain distance, the initiation and termination of the beads are unacceptable due to the non-uniform shape (Fig. 12(a3-a5)).

As shown in Fig. 12b, the bead width decreases as the separation distance increases. This is because as the separation distance increases, energy is lost through conduction, so the melt pool becomes smaller. When the laser then adds more energy again, it has to firstly replace this lost energy to get the melt pool back to the original size generated by the PTA. Any remaining energy then broadens the melt pool. The closer the laser is to the PTA source, then the less the thermal losses are before the addition of the laser energy. Therefore, the bead width gets smaller as the separation distance increases. Based on the presented analysis, the separation distance should be as low as practically possible, which will give a uniform and wide bead appearance. However, if the separation distance is too low, the likelihood of damaging plasma torch by the laser reflection is very high. Therefore, in this study, a minimum separation distance of 10 mm was used.

3.2. Benefits of the hybrid process

3.2.1. Deposition rate

Fig. 13 shows the maximum deposition rates achieved with different applied powers for the PTA and laser processes on their own. It can be seen that the deposition rate increases linearly with the applied power for both processes. Also, for a given power, the deposition rate obtained with PTA is always higher than that of the laser. This is because the beam size of the PTA is smaller than that of the laser (12 mm in this case), and therefore the wire absorbs more power directly from the former heat source. Fig. 14 shows a schematic of the wire under a heat source beam. The power absorbed (P_a) per unit length of wire is the projected area under the beam (width times length of wire exposed) times power density. For round wire, the width is the same as the diameter. Then, P_a can be expressed as:

$$P_a = \eta d D P_d \quad (6)$$

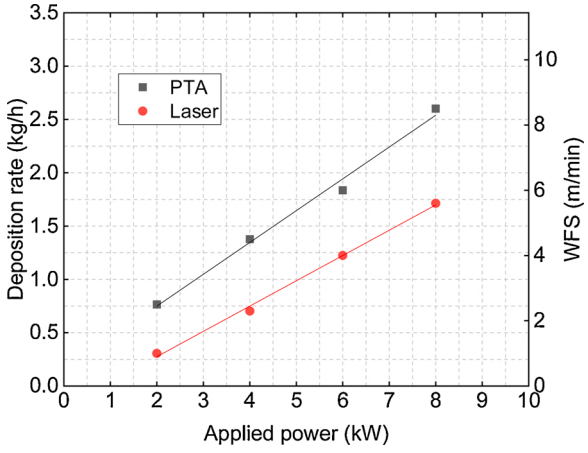


Fig. 13. Comparison of maximum deposition rates obtained with single laser and single PTA processes.

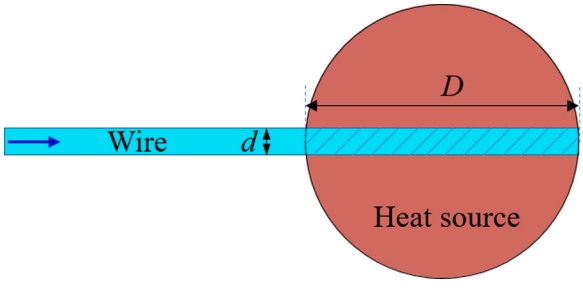


Fig. 14. Schematic shows the wire under a single heat source (PTA or laser). Blue arrow indicates wire feeding direction (For interpretation of the references to colour in this figure legend, the reader is referred to the web version of this article.).

where η is the absorption coefficient, D is the heat source beam diameter, P_d is the power density. P_d is expressed by:

$$P_d = \frac{4P}{\pi D^2} \tag{7}$$

where P is the applied power. By substituting Eq. (7) into Eq. (6), the power absorbed per unit length of wire can be further expressed as:

$$P_a = \frac{4\eta dP}{\pi D} \tag{8}$$

Assuming the same absorption coefficient for the PTA and laser, it can be seen that for the same applied power, more power is absorbed by the wire in the case with smaller beam size. This also means that more power goes to the workpiece with a larger beam size, which is dissipated through thermal conduction. This can be clearly seen from Fig. 15 in that a much wider melt pool was generated with the laser (Fig. 15b) compared to that with the PTA (Fig. 15a) at the same applied power. Actually, if the laser beam size is the same as that of the PTA size, then the difference is solely down to the absorption coefficient. The absorption of laser energy in titanium is quite high (around 0.4) compared to many other metals (e.g., 0.3 for stainless steel and 0.15 for aluminium as measured by Kwon et al. (2012)), but still likely to be lower than PTA on its own (0.5–0.75, as measured by Fuerschbach and Knorovsky (1991)). Therefore, higher deposition rates can be obtained with the PTA compared to that with the laser at the same applied power due to the more direct absorption of energy by the wire from the PTA.

Fig. 16 shows the maximum deposition rates obtained with the hybrid process and compared with PTA only and laser only processes. The total power input for each process is 8 kW, which means that the ratio of power between the laser and the PTA was varied to maintain the same total power in the hybrid process. It can be seen that the maximum deposition rate obtained with the hybrid process was around 0.5 kg/h higher than that of PTA only process (2.6 kg/h), with the lowest deposition rate being the laser only process (1.7 kg/h).

Fig. 17 shows the corresponding hybrid and PTA only deposition processes as presented in Fig. 16. In each case the WFS is the maximum limit for the applied power to achieve a stable process. For the hybrid process, although all three cases have the same total applied power input, the contribution of each heat source for the melting of wire is different in each case. As shown in Fig. 17a, when the arc power is low (2 kW), the PTA preheats the wire but the laser provides most of the energy needed for melting of the wire. In this case, there is no melt pool generated under the arc, and all the melt pool is under the laser. A similar phenomenon occurs in the second case (Fig. 17b), but with hotter wire reaching the laser due to the higher arc power (4 kW). As shown in Fig. 17c, however, at a high arc power of 6 kW, most of the wire is melted by PTA before reaching the melt pool, and the rest of the wire is melted by laser. In this case, the PTA provides a large proportion

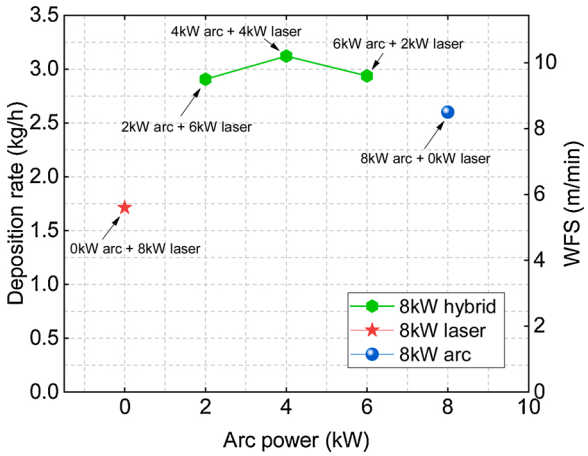


Fig. 16. Comparison of maximum deposition rates obtained with the hybrid process, PTA only process, and laser only process with a total power input of 8 kW in each case.

of energy needed to melt the wire, and there is a melt pool formed under the PTA. As for the PTA only deposition process (Fig. 17d), most of the wire is melted by the arc, and the rest is melted by the melt pool.

The deposition rate of the hybrid process is higher than that of the laser process on its own as it is a combination of the PTA and the laser. For the PTA only process, the deposition rate is limited by the melting of the wire. For a given wire thickness, there is a minimum time for the wire to melt, determined by energy conduction from the top to the bottom. To achieve higher deposition rates, the wire needs to be fed at higher speeds, reducing the effective interaction time for the relatively small PTA. In the hybrid case, the energy distribution is extended and the wire passes into the laser after the arc, and continues to be melted there. It can be seen from Fig. 17 that the melt pools in all the three hybrid cases are longer than that in the PTA only process. Also, Fig. 18 schematically shows the positions of the wire in the hybrid and PTA only processes. It can be seen that both the heat source and the hot melt pool provide energy for the melting of the wire in the two cases. However, the length of the wire surrounded by the heat source and melt pool in the hybrid process (L1 in Fig. 18a) is longer than that in the PTA only process (L2 in Fig. 18b), which gives more time for the energy conduction from the top to the bottom of the wire for the hybrid process, allowing more wire to be melted at the same total applied power. Therefore, compared to the PTA only process, a higher deposition rate was obtained in the hybrid process due to the extended energy distribution and melt pool size.

3.2.2. *Tolerance of WLAM*

As described in Section 3.1.2, the wire is melted by the PTA in the

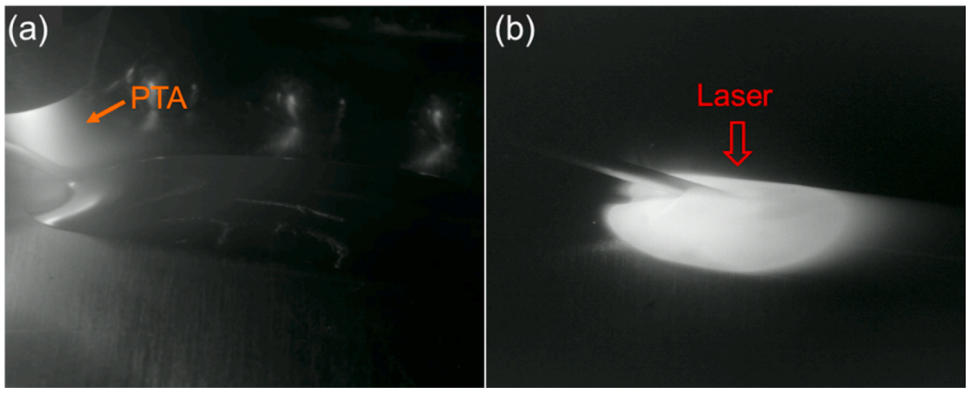


Fig. 15. The deposition processes with the heat source of (a) PTA, and (b) laser, at the same applied power of 6 kW.

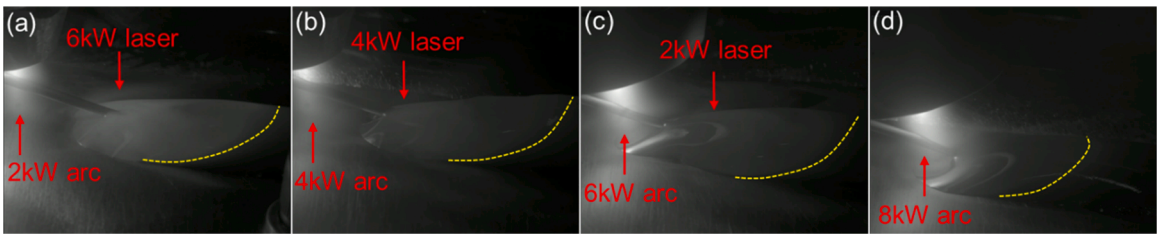


Fig. 17. Hybrid and PTA only deposition process with a total power input of 8 kW: (a) 2 kW arc and 6 kW laser, (b) 4 kW arc and 4 kW laser, (c) 6 kW arc and 2 kW laser, and (d) 8 kW arc. Yellow dashed line indicates the melt pool boundary (For interpretation of the references to colour in this figure legend, the reader is referred to the web version of this article.).

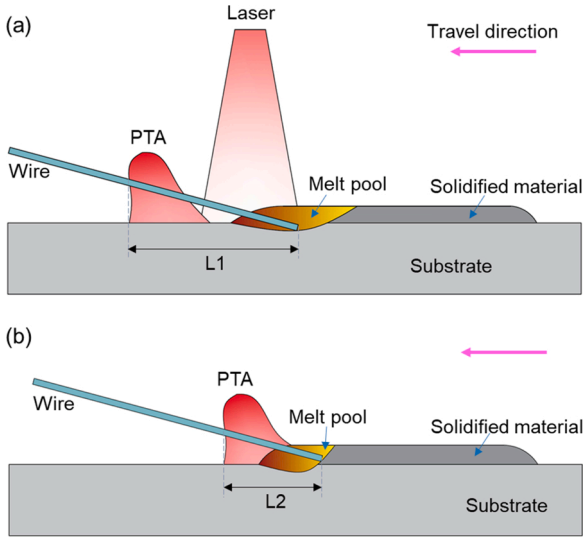


Fig. 18. Schematic shows the positions of the wire in (a) the hybrid PTA-laser process, and (b) single PTA process.

hybrid process, which has a high tolerance and leads to similar bead appearance at different wire feeding positions (Fig. 10). In WLAM, however, the deposition process is very sensitive to the wire feeding position. Fig. 19 shows the deposition processes and the resulting bead appearances at different wire feeding positions. Significant differences in metal transfer mode and bead appearance can be observed at different wire feeding positions. When the wire feeding position was very low ($d_1 = 0$), the wire stabbed the melt pool. This did not cause any major problems but induced irregular oscillations in the melt pool, which is however not reflected on the bead shape. When the distance between the wire tip and workpiece was increased to 1−2 mm, the process was in the optimum configuration, leading to smooth and uniform bead appearances. When this distance was increased further ($d_1 = 3$ mm, $d_1 = 4$ mm), large droplets started to form at the tip of the wire, causing significant oscillations in the melt pool with a fixed period. This is attributed to the high surface tension of titanium and lack of detachment force apart from the gravitational force. This shows that the processing window for the wire feeding position in WALM is very narrow, ranging only from 1 to 2 mm. When the wire position is out of this range, the process is unstable, and deposited beads are unacceptable. Similar phenomena were also reported by Syed et al. (2005); Syed and Li (2005), and Takushima et al. (2020), which indicates the significance of the wire feeding position in WALM. Hence, the hybrid process benefits not only from higher melting efficiency but also from the electromagnetic force of arc and the shear force of plasma gas which helps droplet detachment and does not require the wire to be in direct contact with the melt pool.

3.2.3. Limitation of WAAM

The arc pressure provides a detachment force for the metal transfer, but it also can cause some issues. Wang et al. (2021) reported that the arc pressure increases with the increasing current owing to the increasing electromagnetic force. Above a certain level, a keyhole is formed, which can cause defects in the beads. Fig. 20 shows two deposited beads obtained with two different levels of current. It can be seen that the bead is smooth and uniform at a current of 205 A (Fig. 20a), however when the current is increased to 283 A severe defects are formed, caused by keyhole formation (Fig. 20b). The maximum deposition rate that can be

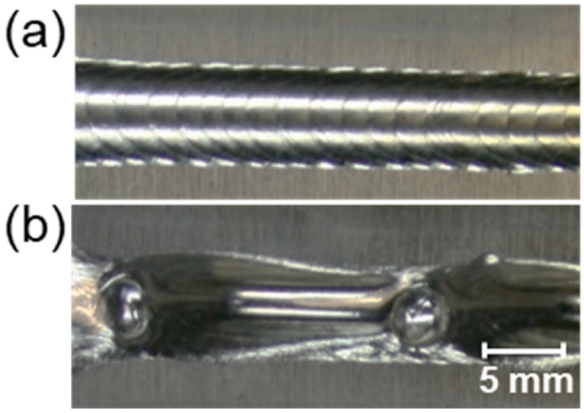


Fig. 20. The effect of current on keyhole formation: (a) bead with a good appearance at 205 A, and (b) bead with defects at 283 A.

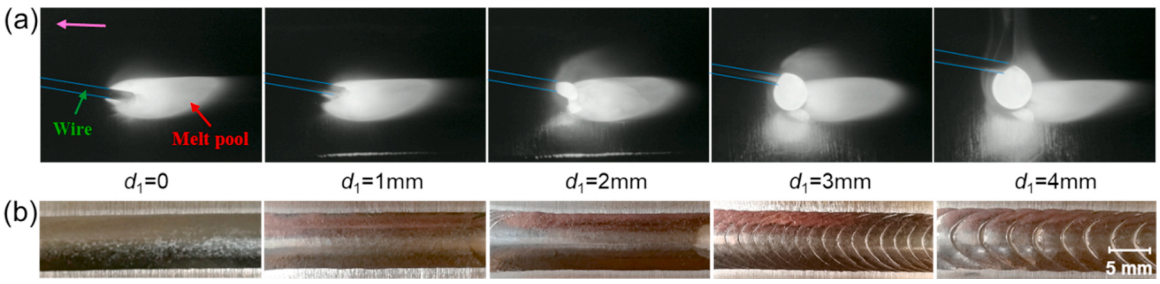


Fig. 19. Tolerance of WLAM to wire-workpiece distance: (a) $d_1 = 0$, (b) $d_1 = 1$ mm, (c) $d_1 = 2$ mm, (d) $d_1 = 3$ mm, and (e) $d_1 = 4$ mm.

achieved with the WAAM process is directly proportional to the arc current. Hence, keyhole formation limits the deposition rate.

Fig. 21 shows the power required for a particular deposition rate and the corresponding beads for WAAM and hybrid processes. The hybrid process can be used as an extension of the WAAM process to increase the deposition rate. At a very low power input (1.67 kW, point A), the energy was just enough to melt the wire, but there was no melt pool generated on the substrate due to the conduction loss, leading to an irregular bead (Fig. 21a). The maximum deposition rate that could be achieved with WAAM process, on the other hand, without any defects was 0.54 kg/h. As the power input exceeded 5.83 kW (point B), keyhole defects started to appear in the melt pool, as shown in Fig. 21b. However, with the same total power input of 5.83 kW (arc power of 4.16 kW and laser power of 1.67 kW), there was no keyhole formed in the hybrid process, and the bead was smooth and uniform (Fig. 21c). For the hybrid process, even with a total power input of 11.67 kW (arc power of 5.83 kW and laser power of 5.84 kW, point C), there still was no keyhole and a regular bead could be formed (Fig. 21d). This means that by adding the laser, the deposition rate could be doubled (from 0.54 to more than 1.08 kg/h in this case) without the risk of keyhole formation.

From the above analysis, one can see that the normal way to improve the deposition rate is increasing the wire feed speed whilst using high energy input. However, with a single PTA heat source, the deposition rate is limited by the keyhole formation due to the high arc pressure at high levels of current. Using the hybrid process, the total applied energy can be distributed to the PTA and laser, which reduces the likelihood of keyhole formation and therefore improves the deposition rate. Another limitation for high deposition rate is the interaction time of the wire with the heat source. If the wire feed speed is too high, there is no enough time for the energy to transfer from the top to the bottom of the wire. However, the extended energy distribution in the hybrid process gives more interaction time for the melting of wire than that in the single PTA or single laser processes, which leads to a higher deposition rate.

In addition, the PTA-laser hybrid AM process combines the advantages of both heat sources. In the hybrid process, the PTA is used to melt the wire and the laser is used to control the melt pool better. Compared to a laser, a PTA has higher efficiency and process tolerance. Therefore, its energy is utilised to initiate the melt pool, melt the wire and ensure efficient metal transfer. Compared to a PTA, a laser in conduction regime does not produce keyhole. Therefore, the laser energy is added to the PTA source, so that a higher deposition rate can be achieved without the generation of keyhole defects.

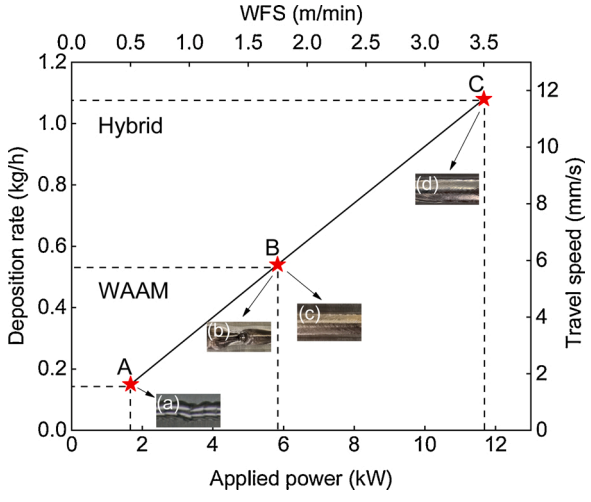


Fig. 21. The deposition rate and bead appearance under different applied powers obtained with WAAM and hybrid processes.

3.3. Multi-layer wall building

Another benefit of the hybrid process should be the independent control of deposition rate and bead shape, leading to a better surface finish. This is because, in WAAM or WLAM, a single axisymmetric heat source (arc or laser) is used simultaneously for melting of feedstock and development of melt pool, which makes the process sensitive to boundary conditions. In the hybrid process, however, two independent heat sources are applied, where the PTA is used to melt the wire and the laser is used to control the melt pool. In this case, we can vary the ratio of energy between both heat sources to change the bead shape and compensate for the change in boundary conditions, whilst maintaining a constant deposition rate. Similarly, the deposition rate can be changed without affecting the bead width. This means that the hybrid process allows independent control of the deposition rate and bead shape.

Fig. 22 shows the cross-sections of the three multi-layer single-pass walls with different widths and deposition rates. The properties of the walls are summarised in Table 4. It can be seen that the achieved flat beads (i.e. high ratio of layer width to height) are very desirable for low surface waviness and lead to a good surface finish, especially wall 1 and wall 2, which have near-net shape. This means that such parts would require little or none post-machining. Also, the relatively high deposition rate of 2.4 kg/h (wall 3) of the hybrid process means shorter deposition time and lower cost of parts compared to the normally used one in WAAM ranging from 0.4 to 1.2 kg/h. In addition, the effective wall width can easily go up to 18.6 mm (wall 3) in the hybrid process. The much higher bead width could be achieved as compared to WAAM process with still better deposition rate and surface quality, meaning that the hybrid process has a larger working envelope than WAAM.

Generally, in WAAM or WLAM processes, the first several layers are narrower than the top layers due to more thermal losses through the substrate (Wu et al., 2017). However, for the single-pass walls built with the hybrid process, the first few layers are slightly wider (Fig. 22). This is because the high heat input of the hybrid process results in relatively large remelting on the pre-existing layers. This makes the melt pool flow down along the lateral wall surfaces (see Fig. 23), which leads to a larger width of the bottom few layers. This means the effective wall width is slightly narrower than the single bead deposited on a plate. In addition, as long as the arc length and the wire feeding position have not been changed, the arc and melt transfer behaviour will not be changed significantly. Fig. 23 shows the deposition process of the first few layers, which exhibits the high stability of the arc and metal transfer behaviour.

3.4. Multi-energy source deposition

As described above, the PTA-laser hybrid AM process has many benefits, but there are some limitations of the process. For DED AM processes, it is very desirable to minimise dilution or remelting ratios. Energy used for melting previous layers is effectively wasted and leads to a very inefficient process. Furthermore, it can cause problems with undesirable microstructures forming and therefore properties if the deposited material goes through many thermal cycles. Finally, it can cause severe problems with residual stresses and distortion. From Fig. 22, it can be seen that the remelting area of the workpiece is significant, which indicates the previous few layers will be remelted when depositing the subsequent layer. This is also indicated by looking at the overall deposition process efficiency. For wall 2, for example, the total power input is 11.4 kW at a deposition rate of 1.8 kg/h, giving a process efficiency of 22.3 MJ/kg for the deposited material. This compares with typical values of 17.0 MJ/kg for a single-pass wall in PTA based WAAM process as demonstrated by Zhang et al. (2017). This is because the highest power density is on the deposit centreline for both the PTA and laser. Thus, much energy is concentrated in the melt pool centreline during the hybrid deposition process.

Fig. 24 shows a comparison of the standard PTA-laser hybrid process and the MES deposition process and the cross-section of the beads

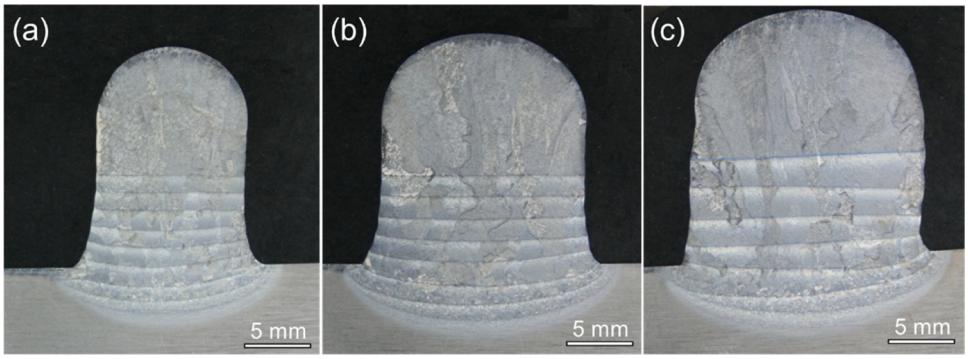


Fig. 22. The cross-sections of the multi-layer single-pass walls at different WFSs showing good surface finish: (a) wall 1: 4 m/min, (b) wall 2: 6 m/min, and (c) wall 3: 8 m/min. The process parameters used are shown in Table 2.

Table 4
Geometric properties of the multi-layer single-pass walls.

Parameters (unit)	Wall 1	Wall 2	Wall 3
Total layer number	10	9	8
Total height (mm)	17.1	18.2	19.8
Average layer height (mm)	1.7	2.0	2.5
Width (mm)	11.5	15.8	18.6
Deposition rate (kg/h)	1.2	1.8	2.4

obtained with the two processes. From Fig. 24 (c) and (d) it can be seen that the bead obtained with the MES process exhibited a wider and shallower profile. It is clear that it will be possible to increase the WFS and therefore to increase the deposition rate and the deposition process efficiency. It can also be seen that both the remelting depth and the heat-affected zone (HAZ) are shallower for the MES process compared to the standard PTA-laser hybrid process. This means the MES process is capable of achieving a high deposition rate and high process efficiency. Further studies of the MES concept will be done in the future.

4. Conclusions

1 For the same applied power, more power can be absorbed directly by the wire from the heat source in the PTA process than in the laser process, giving a higher deposition rate. A higher deposition rate can be achieved for the PTA-laser hybrid process compared to the PTA and laser processes alone. Compared to the laser process, the high deposition rate of the hybrid process is attributed to the combination of the PTA and the laser. Compared to the PTA process, the higher deposition rate is attributed to the extended energy distribution and melt pool size of the hybrid process, allowing higher melting rates for the wire.
2 The deposition rate in the PTA process is limited by keyhole formation, whereas in the hybrid process the range could be significantly expanded by the addition of the laser power. This is due to the lower arc current and hence arc pressure in the hybrid process for the same overall power input.
3 The tolerance to wire positioning of the hybrid process is increased compared to the WLAM process due to the PTA melting the wire.
4 The optimum configuration for the PTA-laser hybrid AM process is PTA leading with the wire fed from the front, giving a stable deposition process as well as a good bead appearance.
5 The separation distance between the laser and arc is very important. Too short distance increases the likelihood of damage of the plasma torch whilst too excessive distance results in narrowing and in certain cases separation of the melt pool into two.
6 By using two heat sources, the hybrid process allows independent control of deposition rate and bead shape. The samples of the multi-layer walls show that the hybrid process can be used for building near-net-shape structures at high deposition rates. The bead width could be controlled in a wide range.
7 The PTA-laser hybrid process has limitations in terms of deposition process efficiency, leading to a high remelting ratio. This is due to there being too much energy on the deposit centreline. To overcome this, a new concept of using a MES was introduced with two laser sources placed either side and just behind the PTA. With this concept, the remelting ratio was significantly improved.

Data Statement

Data underlying this study can be accessed through the Cranfield University repository at https://doi.org/10.17862/cranfield.rd.13806287.

CRediT authorship contribution statement

Chong Wang: Methodology, Validation, Formal analysis, Investigation, Data curation, Writing - original draft, Writing - review & editing, Visualization. **Wojciech Suder:** Conceptualization, Methodology, Formal analysis, Supervision, Writing - review & editing. **Jialuo Ding:** Conceptualization, Methodology, Formal analysis, Supervision, Writing - review & editing. **Stewart Williams:** Conceptualization, Methodology, Writing - review & editing, Supervision, Funding acquisition.

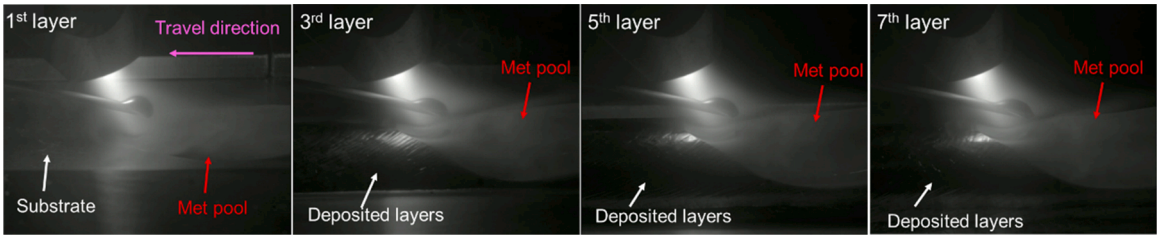


Fig. 23. The deposition process of different layers of wall 2 showing the high stability of the arc and metal transfer behaviour.

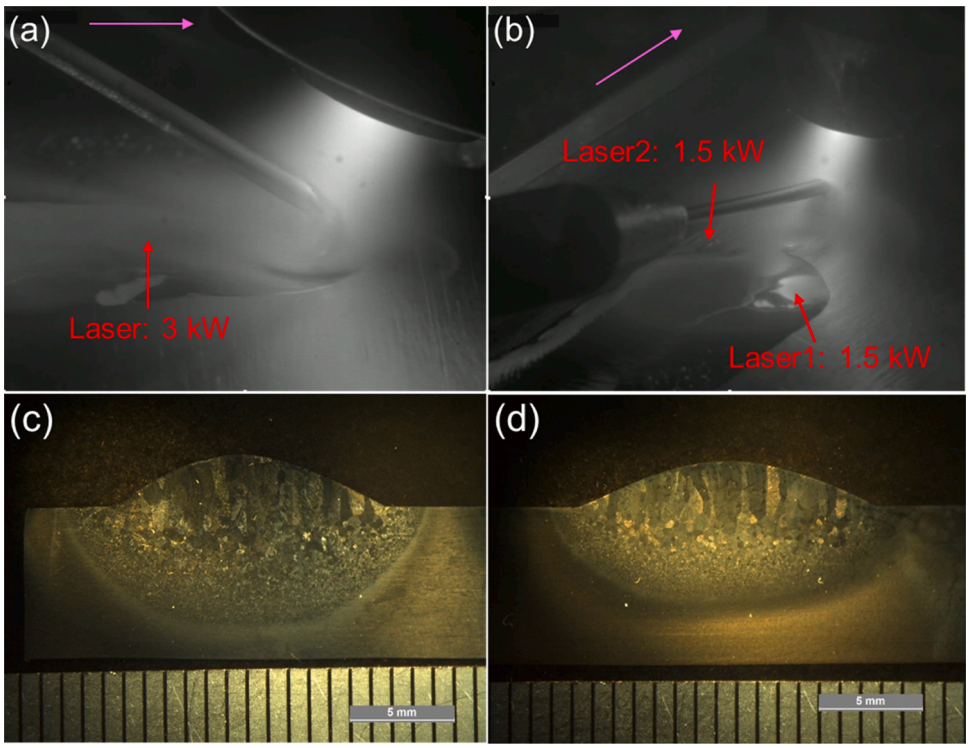


Fig. 24. The deposition process with (a) one PTA (200 A) and one laser (3 kW), and (b) one PTA (200 A) and two lasers (1.5 kW for each laser). (c) and (d) show the cross-section of the deposited beads obtained with the processes in (a) and (b) respectively.

Declaration of Competing Interest

The authors report no declarations of interest.

Acknowledgements

Chong Wang would like to express his gratitude to Welding Engineering and Laser Processing Centre (WELPC) of Cranfield University as well as China Scholarship Council (No. 201706450041) for funding his research studies. The research was also supported by EPSRC funding NEWAM (EP/R027218/1). The authors also would like to thank John Thrower, Nielsen Flemming, Nisar Shah, Steve Pope, and Tracey Roberts for their technical support. In addition, special appreciation goes towards Dr. Jan Hönnige for designing the setup.

References

Baufeld, B., Brandl, E., Van Der Biest, O., 2011. Wire based additive layer manufacturing: Comparison of microstructure and mechanical properties of Ti-6Al-4V components fabricated by laser-beam deposition and shaped metal deposition. J. Mater. Process. Technol. 211, 1146–1158. https://doi.org/10.1016/j.jmatprotec.2011.01.018.

Cong, B., Qi, Z., Qi, B., Sun, H., Zhao, G., Ding, J., 2017. A comparative study of additively manufactured thin wall and block structure with Al-6.3%Cu alloy using cold metal transfer process. Appl. Sci. 7, 1–11. https://doi.org/10.3390/APP7030275.

Fuerschbach, P.W., Knorovsky, G.A., 1991. A study of melting efficiency in plasma - Desconhecido.pdf. Weld. Res. Suppl. 287–297. https://app.aws.org/wj/supplement/WJ_1991_11_s287.pdf.

Kwon, H., Baek, W.K., Kim, M.S., Shin, W.S., Yoh, J.J., 2012. Temperature-dependent absorptance of painted aluminum, stainless steel 304, and titanium for 1.07 μm and 10.6 μm laser beams. Opt. Lasers Eng. 50, 114–121. https://doi.org/10.1016/j.optlaseng.2011.10.001.

Martina, F., Ding, J., Williams, S., Caballero, A., Pardal, G., Quintino, L., 2019. Tandem metal inert gas process for high productivity wire arc additive manufacturing in stainless steel. Addit. Manuf. 25, 545–550. https://doi.org/10.1016/j.addma.2018.11.022.

Miao, Q., Wu, D., Chai, D., Zhan, Y., Bi, G., Niu, F., Ma, G., 2020. Comparative study of microstructure evaluation and mechanical properties of 4043 aluminum alloy fabricated by wire-based additive manufacturing. Mater. Des. 186 https://doi.org/10.1016/j.matdes.2019.108205.

Modenesi, P.J., Nixon, J.H., 1994. Arc instability phenomena in GMA welding. Weld. J. (Miami, Fla) 73, 2195–2245.

Näsström, J., Brückner, F., Kaplan, A.F.H., 2019a. Measuring the effects of a laser beam on melt pool fluctuation in arc additive manufacturing. Rapid Prototyp. J. 25, 488–495. https://doi.org/10.1108/RPJ-01-2018-0033.

Näsström, J., Brueckner, F., Kaplan, A.F.H., 2019b. Laser enhancement of wire arc additive manufacturing. J. Laser Appl. 31, 022307 https://doi.org/10.2351/1.5096111.

Pardal, G., Martina, F., Williams, S., 2019. Laser stabilization of GMAW additive manufacturing of Ti-6Al-4V components. J. Mater. Process. Technol. 272, 1–8. https://doi.org/10.1016/j.jmatprotec.2019.04.036.

Qi, Z., Cong, B., Qi, B., Sun, H., Zhao, G., Ding, J., 2018. Microstructure and mechanical properties of double-wire + arc additively manufactured Al-Cu-Mg alloys. J. Mater. Process. Technol. 255, 347–353. https://doi.org/10.1016/j.jmatprotec.2017.12.019.

Singh, A., Kapil, S., Das, M., 2020. A comprehensive review of the methods and mechanisms for powder feedstock handling in directed energy deposition. Addit. Manuf. 35, 101388 https://doi.org/10.1016/j.addma.2020.101388.

Syed, W.U.H., Li, L., 2005. Effects of wire feeding direction and location in multiple layer diode laser direct metal deposition. Appl. Surf. Sci. 248, 518–524. https://doi.org/10.1016/j.apsusc.2005.03.039.

Syed, W.U.H., Pinkerton, A.J., Li, L., 2005. A comparative study of wire feeding and powder feeding in direct diode laser deposition for rapid prototyping. Appl. Surf. Sci. 247, 268–276. https://doi.org/10.1016/j.apsusc.2005.01.138.

Takushima, S., Morita, D., Shinohara, N., Kawano, H., Mizutani, Y., Takaya, Y., 2020. Optical in-process height measurement system for process control of laser metal-wire deposition. Precis. Eng. 62, 23–29. https://doi.org/10.1016/j.precisioneng.2019.11.007.

Wang, C., Suder, W., Ding, J., Williams, S., 2021. The effect of wire size on high deposition rate wire and plasma arc additive manufacture of Ti-6Al-4V. J. Mater. Process. Tech. 288, 116842. https://doi.org/10.1016/j.jmatprotec.2020.116842.

Williams, S.W., Martina, F., Addison, A.C., Ding, J., Pardal, G., Colegrove, P., 2016. Wire + Arc additive manufacturing. Mater. Sci. Technol. (United Kingdom) 32, 641–647. https://doi.org/10.1179/1743284715Y.0000000073.

Williams, S.W., Suder, W.J., Additive manufacture, Patent, Internaltional publication number: WO 2020/038671 A1.

Wu, B., Ding, D., Pan, Z., Cuiuri, D., Li, H., Han, J., Fei, Z., 2017. Effects of heat accumulation on the arc characteristics and metal transfer behavior in Wire Arc Additive Manufacturing of Ti6Al4V. J. Mater. Process. Tech. 250, 304–312. https://doi.org/10.1016/j.jmatprotec.2017.07.037.

Wu, D., Liu, D., Niu, F., Miao, Q., Zhao, K., Tang, B., Bi, G., Ma, G., 2020. Al–Cu alloy fabricated by novel laser-tungsten inert gas hybrid additive manufacturing. Addit. Manuf. 32, 100954 https://doi.org/10.1016/j.addma.2019.100954.

Zhang, X., Martina, F., Ding, J., Wang, X., Williams, S.W., 2017. Fracture toughness and fatigue crack growth rate properties in wire + arc additive manufactured Ti-6Al-4V. Fatigue Fract. Eng. Mater. Struct. 40, 790–803. https://doi.org/10.1111/ffe.12547.

Zhang, Z., Sun, C., Xu, X., Liu, L., 2018. Surface quality and forming characteristics of thin-wall aluminium alloy parts manufactured by laser assisted MIG arc additive manufacturing. Int. J. Light. Mater. Manuf. 1, 89–95. https://doi.org/10.1016/j.ijlmm.2018.03.005.

DSPACE

https://dspace.org/

Wire based plasma arc and laser hybrid additive manufacture of Ti-6Al-4V

Wang, Chong; Suder, Wojciech; Ding, Jialuo; Williams, Stewart

2021-02-04
Elsevier
https://doi.org/10.1016/j.jmatprotec.2021.117080
Wang C, Suder W, Ding J, Williams S. (2021) Wire based plasma arc and laser hybrid additive manufacture of Ti-6Al-4V. Journal of Materials Processing Technology, Volume 294, July 2021 Article number 117080

Downloaded from a DSpace repository. https://dspace.org/